Melting and Structural Evolution of Palladium and Graphite-supported Palladium Nanoclusters: A Molecular Dynamics Simulation Study

Ling Miao, Venkat R. Bhethanabotla and Babu Joseph
Chemical Engineering Department, University of South Florida,Tampa, Florida 33620-5350

Abstract:

The thermal behavior of palladium nanoclusters of different sizes, in free space and on a graphite surface, was studied using molecular dynamics simulations. The Sutton-Chen many-body potential function was utilized for the metal, and the structured graphite surface was represented by a simple Lennard-Jones model. Changes in thermodynamic and structural properties upon heating and cooling in the temperature range of 300 K to 1400 K were studied. Melting (and wetting, in the graphite-supported case) behavior was characterized by calculating a number of thermodynamic, structural and dynamic properties. Surface melting was found in both cases which developed into the bulk. The energy transfer mechanisms between the pre-melted surface and solid core was studied through calculations of diffusion coefficients in radial shells and the calculation of velocity auto-correlation functions of the atoms in each of these shells.

I. Introduction

The study of melting process and thermodynamic properties of clusters of nanometer length-scales has attracted much theoretical[1,2] and experimental[3,4,5] interest mainly because of their dramatically different behavior from the bulk materials[6]. Transitional and noble metal[7,8,9] or alloy[10,11] clusters are getting more attention, mainly because their extensive applications in catalysts, electronic and opto-electronic nanodevices. Theoretical investigations of their melting phenomena using various simulation methods are focused on the following: (i) The melting temperature and details of the melting process;[12] (ii) the structural evolutions and mechanical properties during heating;[13,14] (iii) the effect of initial structure and size on the melting temperature.[15,16] Cluster melting behavior has often been studied by Monte Carlo and Molecular Dynamics (MD) computer simulations. For example, Chushak and Bartell[12] observed several solid structures to result upon freezing of liquid Au nanoparticles, as a result of the differing kinetics of nucleation and growth, indicating the stochastic nature of the nucleation process, and the possibility of several local minima on the free energy surface; Liu et.al.[17] observed three characteristic time periods, disordering and reordering, surface melting, and overall melting in gold isomers. Lee[18] and his colleagues use the potential energy distribution of atoms in clusters to explain many phenomena related to the phase changes of clusters, which also led to the finding of a new type of premelting mechanism in Pd_{19} cluster.

Pd has a number of fascinating potential applications in heterogeneous catalysis as well as in microelectronic and optoelectronic devices. For example, Pd nanoclusters and nanowires have been used widely in the design of high performance catalysts[19,20] in hydrogenous reactions. Pd is normally supported on a graphite substrate when it is used as a catalyst. Graphite supported Pd is a very effective catalyst in the hydrogenation of nitro-compounds, alkenes, and alkynes.[21] Recently, the significance of the support, on surface area[22] was investigated to improve the catalytic properties of Pd. The structural and dynamic

properties of metallic clusters on graphite surface have also attracted much attention lately.[23,24] Improved experimental techniques, such as scanning tunneling microscopy (STM), low energy cluster beam deposition (LECBD) technique, have provided detailed atomic scale information of the nucleation and growth of atoms on surfaces.[25,26] A nanostructure growth model that incorporates deposition, diffusion, and aggregation was developed by Jensen and co-workers, which describes the diffusion-controlled aggregation exhibited by particles deposited on a surface. Bardotti *et. al*[27] observed rapid movement of large antimony clusters on graphite surfaces, and pointed out that study of these rapid motion mechanisms leads to an understanding of the interaction of nanoparticles with substrates.

Several experiments clearly indicate that quantum behavior of metal nanoclusters is observable, and is most strongly expressed between 1 and 2 nanometers. Hence, particles in that size region should be of most interest.[28] For example, Volokitin[29] found that 2.2 nm Pd clusters show the most significant deviations from bulk behavior at very low temperature compared with those of 3.0, 3.6 and 15nm. Simulation studies of Pd nanoparticle also provide an opportunity for further understanding its unique role in application, and in explaining experimental observations. Although the size of the metallic clusters being simulated ranged from tens to several thousand atoms, most efforts have been focused on size below 150 atoms on both Pd[30] and other metals. In this paper, the melting behavior of free and graphite-supported spherical Pd clusters of 2.3 nm diameter is studied. The support-effect of graphite on both melting and structural properties is investigated in this comparative study. Size-dependence of Pd cluster melting is also investigated.

2. Computational details

Because of the delocalized electrons in metals, the potential functions, which describe the interactions of particles, should account for the repulsive interaction between atomic cores as well as the cohesive force due to the local electron density. Several many-atom potential models were developed during the '80s by various workers, such as Embedded Atom Model,[31] the Glue Model,[32] Tight-binding potential with a second-momentum approximation (TB-SMA),[33] and Sutton_Chen potential model,[34] which was used in our MD simulation. The Sutton-Chen potential can be used to describe the interaction of various metals, such as Ag, Au, Ni, Cu, Pd, Pt, Pb. It is expressed as a summation over atomic positions:

$$U = \varepsilon_{pp} \sum \left(\frac{1}{2} \sum_{j \neq i}^{N} \left(\frac{\sigma_{pp}}{r_{ij}} \right)^{n} - c\sqrt{\rho_i} \right), \tag{1}$$

where $\rho_i = \sum_{j \neq i}^{N} \left(\frac{\sigma_{pp}}{r_{ij}} \right)^{m}$ is a measure of the local particle density. Here r_{ij} is the separation distance between atoms, c is a dimensionless parameter, ε_{pp} is the energy parameter, σ_{pp} is the lattice constant, and m and n are positive integers with $n>m$.

The first term of the expression is a pair-wise repulsive potential, and the second term represents the metallic bonding energy between atomic cores due to the surrounding electrons.

Therefore, it has the same basis as the Finnis-Sinclair potential and introduces an attractive many body contribution into the total energy. This potential can reproduce bulk properties with remarkable accuracy.[35] It provides a reasonable description of small cluster properties for various transition and noble metals.[36,37] S_C potential has also been applied to model the interaction and study the properties of bimetallic alloys, and metal/substrate systems.[11,38,39] Recently, adsorbate effect of supported Pt nanoclusters was studied by S_C potential and was found that the presence of adsorbed atoms stabilizes the surface cluster atoms under an inert gas atmosphere.[40]. Values of S_C parameters for Pd simulations in this paper were taken from the original work of Sutton and Chen[34] as listed in Table 1:

Table 1: Sutton_Chen potential parameters for Pd[1]

σ (Å)	ε (10^{-3} eV)	c	n	m
3.8907	4.1790	108.27	12	7

MD simulations were performed using the DL_POLY[41] package. The system was simulated under canonical (constant NVT) ensemble using the Verlet leapfrog algorithm.[42] Periodic boundary conditions were applied only on the axial direction of the nanowire. No boundary conditions were applied to the cluster. The bulk systems were studied with 3D periodic boundary conditions under constant pressure and temperature (NPT). Both cluster and nanowire were started from face-centered cubic Pd bulk, using spherical cutoff radii to get certain sized ball and cylindrical shapes. The radius of the cluster is defined as[43]

$$R_c = R_g \sqrt{5/3} + R_{Pd}\,, \tag{2}$$

where the atom radius R_{Pd} =1.37Å, R_g is the radius of gyration, given by $R_g{}^2 = \frac{1}{N}\sum_i \left(R_i - R_{cm}\right)$, where $R_i - R_{cm}$ is the distance from center to the coordination point.

A two layer AB stacked graphite substrate with dimensions of 73.8*73.8*6.7Å was used to support Pd clusters. A distance of 2.0Å is set as the initial distance between Pd cluster and graphite. Due to the much smaller carbon-metal interaction forces compared to those for metal-metal, the Lennard-Jones (LJ) potential was deemed adequate to model the Pd-C interactions. Although more accurate and detailed semi-empirical force fields than the Lennard-Jones potential have been reported to provide a reasonable approximation to the behavior of the C-metal systems[44,45] , we feel that adequate representation of the physics is possible within the LJ model used here. The LJ well-depth ε and size σ for C and Pd are listed in Table 2. The Pd-C LJ parameters are calculated using the Lorentz_Berthelot mixing rules.[46] Considering the computational cost, we use a static graphite substrate, where the positions of all C atoms are fixed.

Table 2. Lennard-Jones potential parameters for C and Pd

System	σ (A)	ε (eV)
C-C[47]	3.4	0.002413
Pd-Pd[48]	2.451	0.465
Pd-C	2.9255	0.033497

In all the simulations reported here, a time step of 0.001ps was used. The initial samples, with atoms in ideal FCC positions, were first relaxed by simple quenching followed by annealing cycle. Each system then was then heated with a temperature step of 50K the step size was decreased to 10K when close to melting temperature. Here the cluster adjusts to keep a zero pressure. A cluster size of 2.3 nm with 456 atoms is considered because it has been reported that Pd clusters around this size show the most significant deviations from bulk behavior at very low temperature compared to some other sizes[29] Other size clusters covering a range from tens of atoms to over two thousand atoms are also investigated to find the size effects on melting temperature.

3 Results and discussion

3.1 Melting temperature

The melting transition can be identified in many ways. We first employ the variation of total potential energy and heat capacity with temperature during heating. They are shown in Figure 1. Calculated potential energies increase nearly linearly with temperature at lower temperatures. When close to the transition temperature, simple jumps in total potential energy, indicative of near first order transitions, can be easily observed. According to the potential energy curve, we estimate the melting transition of the unsupported Pd cluster to occur at 1090 K, and that of the supported at 1260 K. In both cases, the Pd cluster has much lower melting temperatures than the bulk, which is 1760K from our simulation. The higher melting temperature of same-sized supported Pd cluster is due to the interaction between Pd and C restraining movement of some of the Pd atoms in the cluster, which also explains the lower potential energies of the supported cluster than the isolated one.

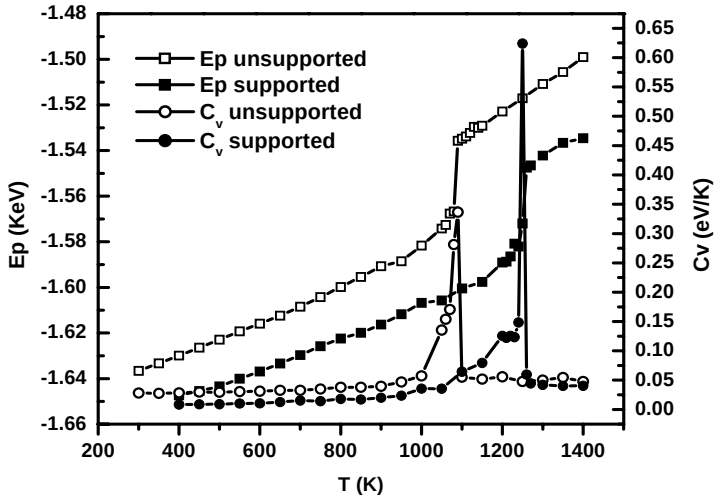

FIG. 1. Potential energy and heat capacity of *d*=2.3 nm supported and unsupported Pd cluster

To further characterize the melting process, the constant-volume specific heat capacity C_v in the canonical ensemble was also calculated. by a standard formula:

$$C_v = \frac{\left\langle (\delta E)^2 \right\rangle}{k_b T^2} = \frac{\left\langle E^2 \right\rangle - \left\langle E \right\rangle^2}{k_b T^2}, \quad (3)$$

where *E* is total potential energy from the heating curve of Figure 1, *N* is number of particles, k_b is the Boltzman constant, and *T* is the temperature. Melting point is defined as the temperature with the maximum apparent heat capacity. The C_v curves in Figure 1 indicate the same melting temperatures as those from *Ep* curves. We observed that the supported cluster has a bit lower heat capacity before melting, but it shows a much larger value at the transition temperature, with much larger fluctuations of the internal energy at the transition point. These differences in thermodynamic properties between supported and un-supported clusters are further characterized using structural and dynamic variables, and are reported later in this paper.

3.2 Analysis of atomic motion

Structural properties and changes in them during heating are of interest in understanding mechanical and catalytic properties of materials. Experimental observations include changes in the lattice parameter, surface coordination number and structural fluctuations. Some theoretical calculations include detailed studies of the topology and structural stability. Small clusters with special numbers of atoms, so-called magic numbers, have proven to be more stable than others.[49] Change in crystallographic structure can be attributed to surface energy. Icosahedral Pd clusters with 13, 55, 147 atoms are examples. The geometry of these extremely small clusters with unique minimum energy has been extensively studied.[13,30] In this work, we pay attention to the time evolution of the structures during heating by investigating two parameters: atomic number distribution along a Cartesian direction and angular correlation functions. The atomic number distribution *N(z)* is defined as

$$N(z) = \left\langle \sum_i \delta(z_i - z) \right\rangle \quad (4)$$

N(z) is a good way to look at the structural features during heating of the supported and un-supported clusters. Plots in Figure 2 describe the distribution of Pd atoms along an axis perpendicular to the graphite surface at different temperatures, where *z=0* is the position of the graphite layer surface in the supported case. We observed that in the solid phase, atoms have higher density only at certain distances from the center, forming many sharp peaks. This is because at low temperatures atoms are oscillating around the lattice sites and retain the crystal-like structure. Those peaks become wider and smaller upon heating, and finally disappear leading to the uniformly distributed atoms in the liquid phase. This expected behavior in *N(z)* is seen in the isolated Pd cluster case, however a different set of *N(z)* distributions for the graphite supported cluster were observed at the corresponding temperatures. We see even at the low temperature of 800K (black dashed lines) the supported Pd cluster has greatly changed its atomic distribution with enhanced peaks close to the

substrate, while still retaining a near spherical shape. This substrate effect is evident even in the weak field of graphite.

The supported Pd cluster continues to stay layered everywhere, with higher density near the surface, at the higher temperature of 1000K (red dashed lines) until it melts. At the melting temperature (blue dashed lines), the entire cluster collapses into a wider ellipsoidal shape, spreading over the substrate with the density reaching essentially zero at 20Å above the substrate. Sharp peaks are evident in the first few monolayers, where the physical state is clearly liquid-like at this melting temperature. Similar density distributions are observed at higher temperatures, with the cluster seen to have essentially melted into a liquid but layered against the surface, as is typically observed in small molecular liquid physisorption. Calculations for the dynamic properties of these Pd atoms as a function of the distance from the surface are underway, and will be reported.

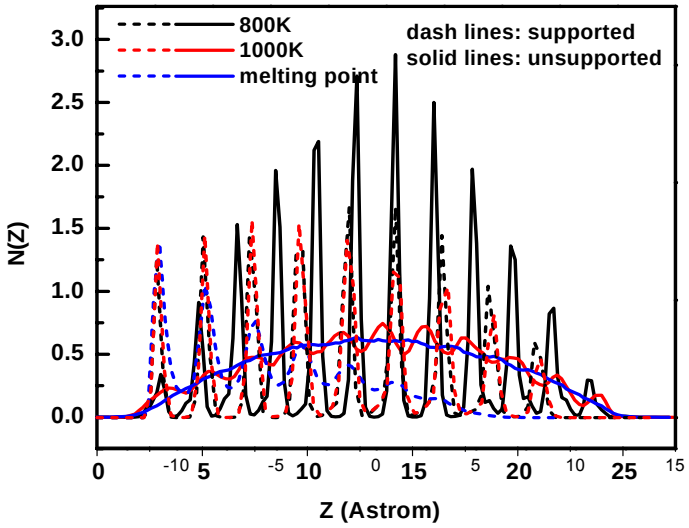

FIG 2 Atomic distribution function along a Cartesian coordinate, which is parallel to the graphite surface for the supported cluster calculations

3.3 Analysis of structural characteristics

To analyze the interior structure of Pd cluster before and after the transition, angular correlation functions were calculated. Angular correlation function (ACF) is an average of angles between a reference atom to its nearest neighbor averaged over all pairs of atoms within a radius R_m from the reference atom [50]. Here R_m is chosen to be the first minimum in the pair correlation function. The angular correlation function is then obtained by approximating the data with a Gaussian with a half width at half maximum (HWHM) of 1°.

ACFs for the un-supported cluster are plotted at different temperatures in Figure 3. At lower temperatures, there are four peaks at 60°, 90°,120°,180° respectively, typical of regular FCC structure. At higher temperatures, the peaks at 90°,180° slowly disappear. When the

entire cluster melts, there are only two major peaks left, which are located around 60° and 120°, showing a hexagonal closed packed structure.

Calculations of the ACFs for the supported clusters are underway and will be reported.

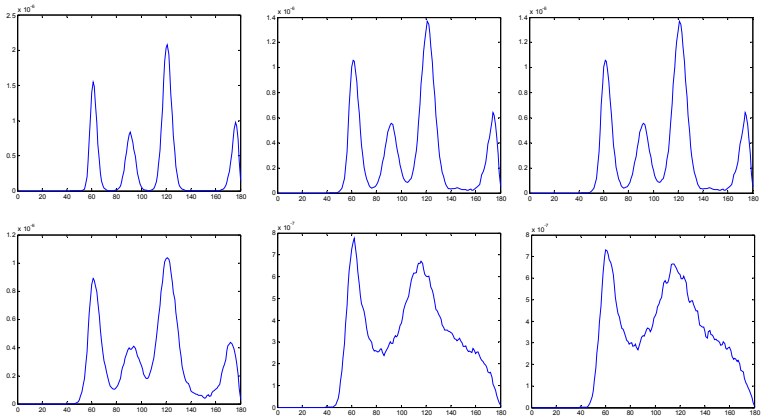

FIG. 3. Angular correlation function for the un-supported Pd clusters at different temperatures. From top left: 400K, 600K, 800K, 1000K, 1100K, 1200K.

4. Conclusions

Molecular dynamics simulations of graphite-supported and unsupported Pd clusters have been carried out in a temperature range that includes surface melting and the homogeneous melting transitions. Surface melting is found in both cases. Calculated thermodynamic properties have revealed differences in surface melting behavior and melting transition temperatures. Density distributions showed significant differences between the free and supported clusters, through the transistion temperature. The supported cluster is seen to melt to a liquid that shows liquid multi-layer physisorbed structure, with sharp density peaks in the first few monolayers. This structure is retained well into the liquid phase past the melting point. Calculated angular correlation functions reveal that this small, unsupported Pd cluster shows a predominantly fcc structure at low temperatures, with some peaks disappearing at higher temperatures. Upon melting, the angular correlation functions reveal a hexagonal close packed structure.

Calculations of angular correlation functions for the supported cluster, and several dynamic properties of both clusters are underway, with the supported cluster properties calculated in the physisorbed layers, as a function of distance form the substrate. These results will be reported at the meeting in addition to the above.

Acknowledgement

Partial support was provided by NASA-Glenn via FSEC, Florida. The Daresbury Laboratory provided the DL_POLY package and Academic Computing at the University of South Florida provided computational resources, both of which are gratefully acknowledged. The authors thank Subramanian K.R.S.S. for some valuable discussions.

References

1 M. Schmidt, R. Kusche, W. Kronmüller, B. V. Issendorff, and H. Haberland, Phys.Rev.Lett.**79**, 99 (1997).
2 F. Ercolessi, W. Andreoni, and E. Tosatti, Phys. Rev. Lett. **66**, 911 (1991).
3 M M. Schmidt, R. Kusche, W. Kronmüller, B. V. Issendorff, and H. Haberland, Nature **393**, 238 (1998).
4 S. L. Lai et al., Phys. Rev. Lett. **77**, 99 (1996).
5 K. F. Peters, J. B. Cohen, and Y-W Chung, Phys. Rev. B **57**, 13430 (1998).
6 R. R. Couchman, Phil. Mag. A **40**, 637 (1979).
7 R. C. Longo, Surf. Sci. **459**, L441 (2000).
8 T. X. Li, Y. L. Ji, S. W. Yu, and G. H. Wang, Solid State Comm. **116**, 547 (2000).
9 C. Rey, L. J. Gallego, G. J. Rodeja, J. A. Alonso and M. P. Iniguez, Phys. Rev. B **48**, 8253 (1993).
10 Y Shimizu, K. S. Ikeda, and S. Sawada, Phys. Rev. B **64**, 075412 (2001).
11 S. Huang, and P. B. Balbuena, J. Phys. Chem.B **106**, 7225 (2002).
12 Y. G. Chushak, and L. S. Bartell, J. Phys. Chem. B **105**, 11605 (2001).
13 C. L. Cleveland, W. D. Luedtke, and U. Landman, Phys. Rev. B **60**, 5065 (1999).
14 J-P. Borel, Surf.Sci. **106**,1 (1981).
15 Ph. Buffat, and J-P. Borel, Phys. Rev. A, **13**, 2287, (1976)
16 F. Ercolessi, W Andreoni, and E. Tosatti, Phys. Rev. Lett. **66**, 911 (1991).
17 H. B. Liu, J. A. Ascencio, M. P. Alvarez, and M. J. Yacaman, Surf. Sci. **491**, 88 (2001).
18 Y. J. Lee, E. K. Lee, and S. Kim Phys. Rev. Lett. **86,** 999, (2001).
19 G. Schmid, S. Emde, V. Maihack, W. Meyer-Zaika, and St. Peschel, J. Mole. Catal. A **107**, 95 (1996).
20 H-U. Blaser, A. Indolese, A. Schnyder, H. Steiner and M. Studer, J. Mole. Catal. A. **173,** 3 (2001)
21 D. Savoia, C., Trombini, A. Umani-Ronchi, and G. Verardo, J. Chem. Soc., Chem. Commu. **11**, 504 (1981).
22 G. Farkas, L. Hegedus, A. Tungler, T. Mathe, J. L. Figueiredo, and M. Freitas, J. Mol. Catal. A **153**, 215 (2000).
23 D. Bazin, Topics Catal. **18**, 79 (2002).
24 S-P Huang, D. S. Mainardi, and P. B. Balbuena, Surf. Sci. **545**, 163 (2003).
25 G. S. Bales, and D. C. Chrzan, Phys. Rev. B **50**, 6057 (1994).
26 P. Melinon, P. Jensen, J. X. Hu, A. Hoareau, B. Cabaud, M. Treilleux, and D. Guillot, Phys. Rev. B **44**, 12562, (1991).
27 L. Bardotti, P. Jensen, A. Hoareau, M. Treilleux, and B. Cabaud, Phys. Rev. Lett. **74**, 4694 (1995).
28 G. Schmid, M. Baumle, M. Geerkens, I. Helm, C. Osemann, and T. Sawitowski, Chem. Soc. Rev. **28**, 3 (1999).
29 Y. Volokitin, J. Sinzig, L. J. deJongh, G. Schmid, M. N. Vargaftik, and II. Moiseev, Nature **384,** 621 (1996).
30 J.Westergren, and S. Nordholm, Chem. Phys. **209**, 189 (2003)
31 S. M. Foiles, M. I. Baskes, and M. S. Daw, Phys. Rev. B **33**, 7983 (1986).
32 F. Ercolessi, E. Tosatti, and M. Parrinello, Philos. Mag. A **58**, 213 (1988); Phys. Rev. Lett. **57**, 719 (1986).
33 D. Tomanek, A. A. Aligia, and C. A. Balseiro, Phys. Rev. B **32**, 5051 (1985).
34 A. P. Sutton, and J. Chen, Phil. Mag. Lett. **61**,139 (1990).
35 J Uppenbrink, and D. J. Wales, J. Chem. Phys. **98**, 5720 (1993).
36 D. J. Wales, and L. J. Munro, J. Phys. Chem. **100**, 2053 (1996).
37 L. D. Lloyd and R. L. Johnston, Dalton **3**, 307 (2000).
38 Z. A. Kaszkur and B. Mierzwa, Phil. Mag. A **77**, 781 (1998).
39 J. A. Nieminen, Phys. Rev. Lett. **74**, 3856 (1995).
40 E. J. Lamas, P. B. Balbuena. J. Phys. Chem. B 107, 42 (2003).
41 W. Smith, and T. R. Forester, DL_POLY; Daresbury Laboratory, Daresbury, UK, 1996.
42 M. P. Allen, and D. J. TIldesley, *Computer simulation of liquids, Clarendon Press*, (Oxford, 1987), P80.
43 L. Wang, Y. Zhang, X. Bian, and Y. Chen, Phys. Lett. A **310**, 197 (2003).
44 S. Y. Liem and K–Y. Chan, Surf. Sci. **328**, 119 (1998).
45 H. Rafii_Tabar, H. Kamiyama, and M. Cross, Surf. Sci. **385**, 187 (1997).
46 D. Frenkel and B. Smit, Understanding of molecular simulation. Academic Press, San Diego, 1996.
47 V. R. Bhethanabotla, and W.A. Steele Phys. Rev. B **41**, 9480 (1990).
48 P. M. Agrawal, B.M. Rice, and D. L. Thompson, Surf. Sci. **515**, 21 (2002).
49 O. Echt, K. Sattler and E. Recknagel, Phys. Rev. Lett, **47**, 1121 (1981).
50 E. Ko, M. Jain, and J. R. Chelikowsky, J. Chem. Phys. **117**, 1476 (2002).